Atomistic Simulation of the Sorption of Small Gas Molecules in Polyisobutylene

Georgia Tsolou and Vlasis G. Mavrantzas*

Department of Chemical Engineering, University of Patras & Institute of Chemical Engineering and High-Temperature Chemical Processes (FORTH-ICE/HT), Patras GR-26504, Greece

Zoi A. Makrodimitri and Ioannis G. Economou

Molecular Thermodynamics and Modeling of Materials Laboratory, Institute of Physical Chemistry, National Center for Scientific Research "Demokritos", GR-15310 Aghia Paraskevi Attikis, Greece

Rafiqul Gani

CAPEC, Department of Chemical and Biochemical Engineering, Technical University of Denmark, DK-2800 Lyngby, Denmark

Received April 5, 2008; Revised Manuscript Received June 13, 2008

ABSTRACT: Polyisobutylene (PIB), an important elastomer with a low glass transition temperature, presents markedly low permeability properties to small-molecule penetrants compared to other elastomers. In the past, computer simulation approaches to explain this behavior have led to diffusivity and solubility calculations that, unfortunately, deviated significantly from the experimental values. We present here the results of a new simulation strategy which leads to accurate predictions of the solubility of four gases (He, Ar, N_2, and O_2) in PIB, thus opening up the way toward understanding the molecular origin of the superior barrier properties of PIB. A critical element in the new approach is the introduction of a reliable united-atom model for PIB that can accurately reproduce its conformational characteristics and volumetric properties over a wide range of temperature conditions, thereby providing well-equilibrated representative PIB structures for subsequent permeability studies with a more accurate force field. To this, independent PIB configurations thoroughly pre-equilibrated with the new model are converted to all-atom PIB structures, re-equilibrated using the detailed COMPASS force field, and employed in a series of sorption runs for the estimation of the infinite dilution solubility coefficient, S_0, of the small gas molecules. Simulation results for the solubility of He, Ar, N_2, and O_2 in PIB at room temperature are found to reproduce experimental data with very good accuracy. Additional results at progressively higher temperatures show that the solubility of O_2 and Ar is always higher than that of N_2 and He, respectively. We also find that calculations based on a united-atom representation overestimate systematically the solubility of these gases, with the exception of He.

1. Introduction

Polyisobutylene (PIB), whose chemical structure is of the form $CH_3-[C(CH_3)_2CH_2]_x-H$, belongs to the class of symmetrically substituted vinylidene polymers that have been studied extensively in the recent past since they possess a number of interesting properties over their vinyl counterparts.[1–41] For example, PIB is characterized by a low glass transition temperature (it is the least fragile polymer or a strong liquid[1] in Angell's terminology[2]) even though the presence of the bulky pendant methyl groups hinders segmental mobility with respect to skeletal bond rotations, rendering it an elastomeric material. With respect to other elastomers, on the other hand, it exhibits low permeability to small-molecule penetrants such as air and light gases, which has been attributed to its higher density.[3] Today, PIB finds numerous applications in rubber technology, in lubrication, even in biomedical engineering.[4]

The conformational, structural, and dynamic properties of PIB over a range of temperature and pressure conditions have experimentally been studied with several state-of-the art techniques such as X-ray[5–8] and neutron scattering (NS),[9–11] neutron spin echo (NSE),[12,13] dynamic light scattering,[14] dielectric spectroscopy (DS),[15,16] nuclear magnetic resonance (NMR),[17–21] photon correlation spectroscopy,[22] positron lifetime experiments,[23] and rheological measurements.[24–26] Theoretical studies, on the other hand, such as the calculations of Hoeve[27] and Madkour et al.,[28] the elaborate calculations of Boyd and Breitling[29] on the conformational properties of model PIB compounds for the most stable conformation, the detailed studies of Suter et al.[30,31] for the effect of steric strain on the configuration of a long-chain PIB molecule with the rotational isomeric state (RIS) model, and the Monte Carlo simulations of Vacatello and Yoon,[32] have provided invaluable information about the conformational characteristics of PIB. Today, it is generally accepted that, to a very good approximation, the equilibrium values for the skeletal bond angles are approximately equal to 126° at the methylene groups and equal to 110° (tetrahedral value) at the quaternary carbon atoms, while the distribution of torsional angles exhibits six distinct minima centered at +15° (t_+), −15° (t_-), +130° ($g^{\pm}$), +105° (g^{+}), −105° ($g^{\mp}$), and −130° (g^{-}). On the basis of a six-state RIS model, calculated values of the characteristic ratio at infinite chain length have been in very good agreement with experimental data, while the polymer reference interaction site model (PRISM) reproduces quite accurately X-ray-based experimental data.[6,7]

Of interest are also the recent molecular dynamics (MD) simulation studies of Karatasos et al.[20,33,34] on the segmental dynamics in bulk PIB and, in particular, on the coupling between methyl rotation and backbone motion and its connection to the dielectric β-relaxation.

* To whom correspondence should be addressed: e-mail vlasis@chemeng.upatras.gr, tel +30-2610-997-398, fax +30-2610-965-223.

10.1021/ma8007652 CCC: $40.75
Published on Web 08/02/2008

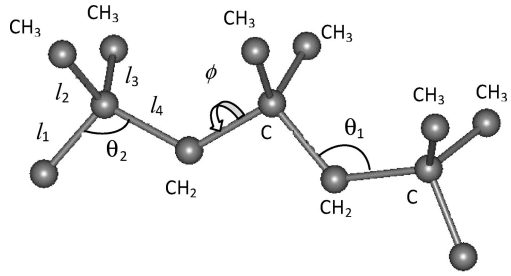

Figure 1. United-atom representation of PIB.

The literature survey reveals that most of the simulation studies on PIB[3,32,35–41] have been limited to rather short-chain and small-size systems. For example, the longest simulated PIB system so far comprises 100 atoms per molecule, while the duration of the MD simulation did not exceed 10 ns.[38] It is also true that, in addition to pendant methyl dynamics and β-relaxation, most of the simulation efforts have been restricted to the study of the volumetric and conformational properties of PIB as well as to the diffusion of a small penetrant (e.g., methane, CH_4) through its amorphous matrix.

The main objective of this work is to extend these studies to longer chain systems through the development of a reliable united-atom (UA) force field for PIB which will permit accessing simulation times significantly longer than what is possible with all-atom (AA) models. We introduce such a force field here and exhaustively validate it against known results for a number of PIB systems concerning volumetric, structural, and conformational properties and their dependence on chain length. Further, configurations thoroughly pre-equilibrated with the new force field are used as input to AA model simulations in order to calculate the solubility of four small gases, namely, helium (He), argon (Ar), oxygen (O_2), and nitrogen (N_2), in PIB at various temperatures. A reliable UA model for PIB is a major achievement because it will further help in predicting the viscoelastic properties of this polymer, such as the zero shear viscosity and its variation with chain length, the monomer friction coefficient, the interentanglement spacing, and the plateau modulus. No such data have been reported for PIB so far from molecular simulations.

The paper is organized as follows: Section 2 describes in detail the new UA molecular model for PIB and the details (chain length, size, temperature) of the systems examined. Simulation results concerning the thermodynamic, conformational, and structural properties that validate the new model are presented in section 3. Section 4 outlines the methodology used to calculate the solubility of the four small gas molecules in PIB and the results obtained. The major findings of the present work and future plans are discussed in section 5.

2. Molecular Model and Systems Examined

In the UA model considered here for PIB (see Figure 1), the lengths of all bonds in a PIB monomer (i.e., the bonds denoted as l_1, l_2, and l_3 in Figure 1) are considered constant and equal to 1.54 Å, while the length of the bond connecting two adjacent monomers along the PIB chain backbone (denoted as l_4 in Figure 1) is allowed to fluctuate according to a harmonic bond-stretching interaction of the form

$$U_{str} = k_{str}(l - l_0)^2 \tag{1}$$

The parameters k_{str} and l_0 denote the stiffness and equilibrium length of the bond, respectively, and their values are listed in Table 1a. They have been chosen so as to prevent unphysical distortion of the bond from the large stresses generated in PIB structures due to methyl crowding. Consequently, k_{str} has been taken twice as large the value proposed by Nath and Khare,[42] while l_0 has been chosen equal to 1.50 Å, very close to the value proposed by Gee and Boyd[43] for the methine−methylene interaction in a polybutadiene (PB) monomer. With such a parametrization, and due to the strong methyl−methyl interactions, the average value of l_4 comes out to be 1.54 Å, i.e., exactly equal to the fixed value chosen for the bond l_1 (as it should, given the equivalence of the two bonds based on symmetry arguments). This was impossible to achieve with the parametrizations proposed by Pütz et al.[7] and Nath and Khare[42] using the NERD model expressions and parameter values for the nonbonded interactions. Significant deviations of the average value of the l_4 bond form the desired value of 1.54 Å were also observed when a very stiff value was used for the spring constant in conjunction with values for the parameters describing nonbonded interactions based on the TRAPPE model.[7,44]

Table 1. (a) Parameters for the Stretching, Bending (Taken from Refs 42 and 44), and Torsional (Taken from Ref 34) Interactions in PIB; (b) Parameter Values for the Nonbonded LJ Interactions in PIB According to the New UA Model Introduced in This Work (Taken from Refs 42, 44, and 45) and Comparison with the Corresponding Values in the Known NERD[42] and TraPPE-UA[44] Potential Models

(a) Stretching

bond	k_{str} (kcal mol^{-1} Å^{-2})	l_0 (Å)
CH_2−C (l_1)	infinitely stiff	1.54
C−CH_3 (l_2)	infinitely stiff	1.54
C−CH_3 (l_3)	infinitely stiff	1.54
C−CH_2 (l_4)	192.0	1.50

Bending

bond angle	k_θ (kcal mol^{-1} rad^{-2})	θ_0 (deg)
CH_3−C−CH_3 (θ_2)	124.2	109.47
CH_2−C−CH_3(θ_2)	124.2	109.47
CH_2−C−CH_2 (θ_2)	124.2	109.47
C−CH_2−C (θ_1)	124.2	114.0

Torsional

dihedral	k_ϕ (kcal mol^{-1})
CH_2−C−CH_2−C	2.8

(b) Nonbonded LJ

	current work		TraPPE-UA		NERD	
site	ε (kcal mol^{-1})	σ (Å)	ε (kcal mol^{-1})	σ (Å)	ε (kcal mol^{-1})	σ (Å)
C	0.018	2.44	0.00099	6.40	0.00337	3.91
CH_2	0.091	3.95	0.091	3.95	0.091	3.93
CH_3	0.199	3.825	0.195	3.75	0.139	3.85

A harmonic potential of the form

$$U_\theta = \frac{1}{2}k_\theta(\theta - \theta_0)^2 \tag{2}$$

is assumed to describe the potential energy associated with the deformation of the two skeletal bond angles at the methylene and quaternary groups, denoted as θ_1 and θ_2 in Figure 1, respectively. The parameters k_θ and θ_0 are taken from Martin and Siepmann,[44] and their values are also listed in Table 1a.

Intramolecular interactions associated with dihedral angles along the PIB chain backbone (angle ϕ in Figure 1) are described by a torsional energy function of the form

$$U_\phi = \frac{1}{2}k_\phi(1 - \cos 3\phi) \tag{3}$$

as suggested by Karatasos et al.;[33,34] the value of the parameter k_ϕ is reported in Table 1a.

All nonbonded interactions (intermolecular and intramolecular between atoms separated by more than three bonds) are

estimated using the traditional 6−12 Lennard-Jones (LJ) potential:

$$U_{LJ} = 4\varepsilon_{ij}\left[\left(\frac{\sigma_{ij}}{r_{ij}}\right)^{12} - \left(\frac{\sigma_{ij}}{r_{ij}}\right)^{6}\right] \quad (4)$$

with i and j denoting the different types of LJ sites occurring in PIB (C, CH_2, and CH_3). The corresponding ε and σ values are listed in Table 1b and are seen to differ from those proposed by Nath and Khare[42] and Martin and Seipmann.[44] Again, this choice was dictated by the fact that these other values failed to reproduce the PIB melt density accurately, the correct dihedral angle distribution, and the well-established splitting of the trans and gauche states in PIB, especially at the higher temperatures; thus, they were not considered any further. A key to the correct sampling of the six rotational isomeric states have been the values assigned to parameters ε and σ for the quaternary carbon site, which have been taken from Poncela et al.[45]

Standard Lorentz−Bethelot combining rules have been used for the calculation of the LJ parameters between pairs of unlike atoms, with the cutoff distance set in all cases equal to 12 Å as proposed by Pütz et al.[7]

Using this UA model, a number of monodisperse PIB systems were simulated in the *NPT* statistical ensemble at several temperatures above the melting point. Specific details of the simulated systems with respect to number of total carbon atoms per chain, number of chains, total number of atoms in each system, and temperature are reported in Table 2. For all systems, the initial configuration was created using the Materials Studio software package[46] followed by a potential energy minimization procedure and exhaustive pre-equilibration via a long *NVT* MD simulation run at 450 K, at a density value close to the experimental one at this temperature. All results reported here have been obtained by long *NPT* MD simulations at 0.1 MPa and at several temperatures in the range 300−600 K, starting always from a fully equilibrated system configuration at 450 K. The Nosé-Hoover thermostat−barostat[47,48] was used in order to maintain temperature and pressure at their prescribed values. Constraint forces associated with fixed lengths for the l_1, l_2, and l_3 bonds in all PIB monomers were determined using the SHAKE−RATTLE algorithm.[49,50] The equations of motion were integrated using a single time step equal to 2 fs. The duration of the MD production runs varied from 10 ns (in the case of the shorter chain systems and higher temperatures) to 300 ns (in the case of the longer systems and lower temperatures). All simulation runs were carried out using the parallel molecular dynamics software LAMMPS.[51]

3. Results

3.1. System Equilibration. In Figure 2a, MD results are shown concerning equilibration of the C_{80} PIB system at three different temperatures, namely 350, 450, and 550 K, in terms of the decay of the time autocorrelation function $\langle \mathbf{u}(t)\cdot\mathbf{u}(0)\rangle$ for the unit vector $\mathbf{u}$ directed along the chain end-to-end vector. Figure 2b refers to the evolution of the mean square chain end-to-end distance, $\langle R^2\rangle$, in two of the simulated systems (C_{80} and C_{120}) with time t. In all cases, the function $\langle \mathbf{u}(t)\cdot\mathbf{u}(0)\rangle$ is seen to decay to zero after a certain time, which depends strongly on T. This is true even for the lower temperature of 350 K where the $\langle \mathbf{u}(t)\cdot\mathbf{u}(0)\rangle$ function is seen to drop to zero rather slowly corresponding to a relaxation time of about 100 ns (as compared to about 5 ns for the same system at 450 K). This fast rise of the relaxation time with decreasing temperature is indicative of the difficulties faced by brute-force MD simulations in sampling the terminal relaxation properties of polymers in their submelt regime. $\langle R^2\rangle$ is also seen to relax to well-defined values, characteristic of a fully equilibrated system, for all temperatures examined. Similar behavior was obtained for the rest of the PIB systems simulated here whose relaxation is faster or slower compared to C_{80} at the same temperature, in accordance with the predictions of well-established theories, such as the Rouse, the modified Rouse, and the reptation, for the chain length dependence of terminal relaxation.

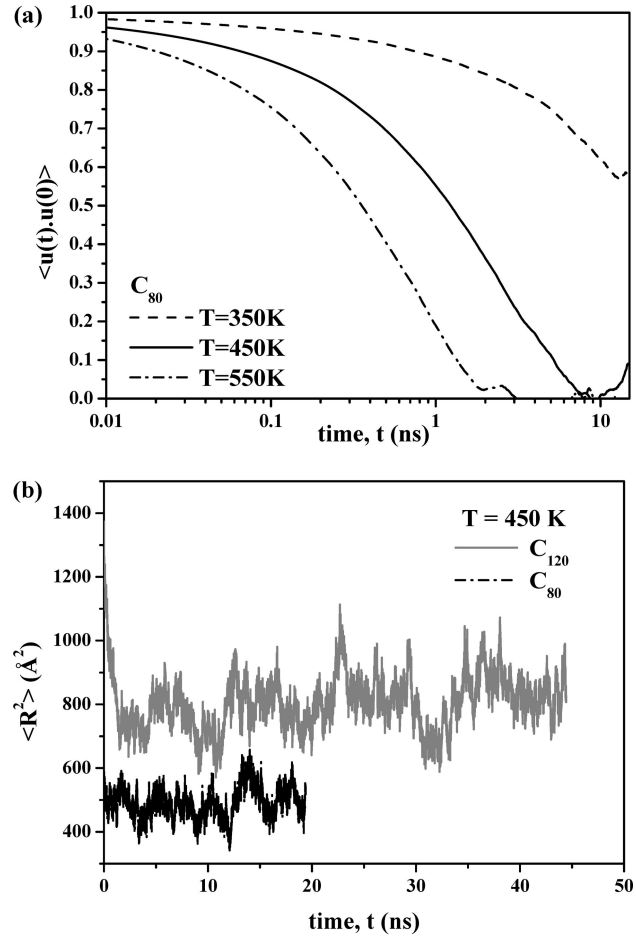

Figure 2. (a) Time decay of the autocorrelation function of the chain end-to-end unit vector, $\langle \mathbf{u}(t)\cdot\mathbf{u}(0)\rangle$, corresponding to the C_{80} system at 350, 450, and 550 K. (b) Evolution of the instantaneous value of the average chain end-to-end distance, $\langle R^2\rangle$, with time t as obtained from the present MD simulations with the C_{80} and C_{120} systems at 450 K.

Table 2. Details of the Simulated PIB Systems

system	no. of carbon atoms per chain	no. of chains	total no. of atoms	temperature (K)
C_{32}	32	120	3072	450
C_{48}	48	80	3840	450
C_{64}	64	64	4096	450
C_{80}	80	40	3200	300, 350, 400, 450, 500, 550
C_{100}	100	40	4000	450
C_{120}	120	32	3840	450
C_{140}	140	32	4480	450
C_{160}	160	32	5120	450
C_{200}	200	32	6400	450
C_{240}	240	32	7680	300, 350, 400, 450, 500, 550, 600
C_{320}	320	24	7680	300, 350, 400, 450, 500, 550

3.2. Conformational Properties. A critical test for the new UA force field introduced in this work concerns its accuracy in reproducing the conformational properties of PIB melt as quantified by the distributions of bond lengths, bending angles, dihedral angles and chain dimension parameters such as the average chain end-to-end distance, the radius of gyration, and

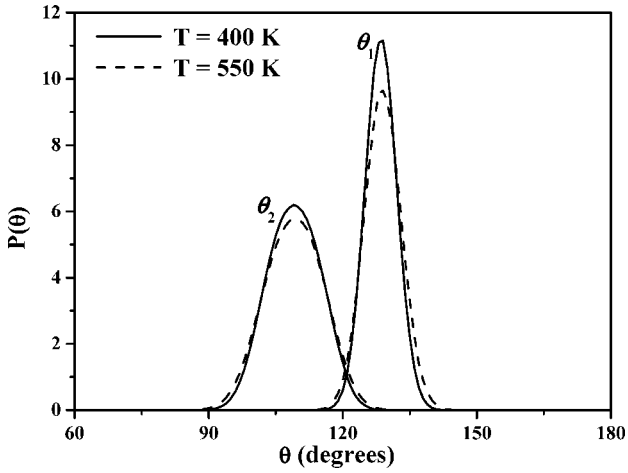

Figure 3. Distribution of the two backbone bond angles θ_1 and θ_2 (see Figure 1) at two different temperatures.

the characteristic ratio. In Figure 3, the probability distribution of the population in the two bending angles along the backbone of a PIB chain (i.e., at the CH_2 atoms marked as θ_1, and at the disubstituted C atoms marked as θ_2 in Figure 1) at two different temperatures is shown. The two distributions are practically Gaussian and are characterized by different mean values and widths. The bond angle centered at the quaternary carbon, θ_2, exhibits a broader distribution around an equilibrium value of 109.5° (i.e., very close to the tetrahedal angle), while the methylene centered angle, θ_1, is more narrow with a peak at a significantly larger value (128.5°) due to the steric strain generated by the strong repulsive interactions between adjacent methyl units. These results, which are found to be independent of the chain length, agree very favorably with the X-ray diffraction measurements of Tanaka et al.[52] for the crystal structure of PIB which yielded average values for the skeletal θ_2 and θ_1 bond angles equal to 110° and 128°, respectively. They are also consistent with the MD simulation results of Karatasos et al.[33,34] based on an AA model for the distribution of skeletal angles in the central portion of the PIB chains. Figure 3 also shows that as the temperature increases the two curves broaden up but their average or equilibrium values remain unaltered.

The distribution of torsion angles, ϕ, at two different temperatures of 350 and 450 K is shown in Figure 4a. It clearly exhibits six characteristic maxima at ±15° corresponding to the two trans conformational states (t^+ and t^-) and at ±107° and ±128° corresponding to the two gauche conformational states (g^+ and g^-) and their splitting, which is more pronounced at the lower temperatures. These results, which are also consistent with the MD simulation results of Karatasos et al.[33,34] based on an AA model, confirm the elaborate calculations of Boyd and Breilding[29] and the Monte Carlo simulations of Vacatello and Yoon[32] that the potential energy hypersurface of model PIB compounds should be described by a six-state RIS model. The locations of the peaks are also consistent with the calculations of Suter et al.[30,31] for the positions of the rotational isomeric states (RIS) in PIB based on an iterative method that eliminates end effects in RIS calculations for short chains, thus correctly estimating the effects of steric strain on configuration. The splitting of the three conformational states becomes more pronounced as the temperature decreases, although their positions remain unaffected.

The capability of the UA force field introduced in the present study to successfully reproduce the distribution of the torsion angles, ϕ, is a significant accomplishment. As mentioned above, this was impossible to achieve with known and widely used UA models models reported in the literature for hydrocarbons.

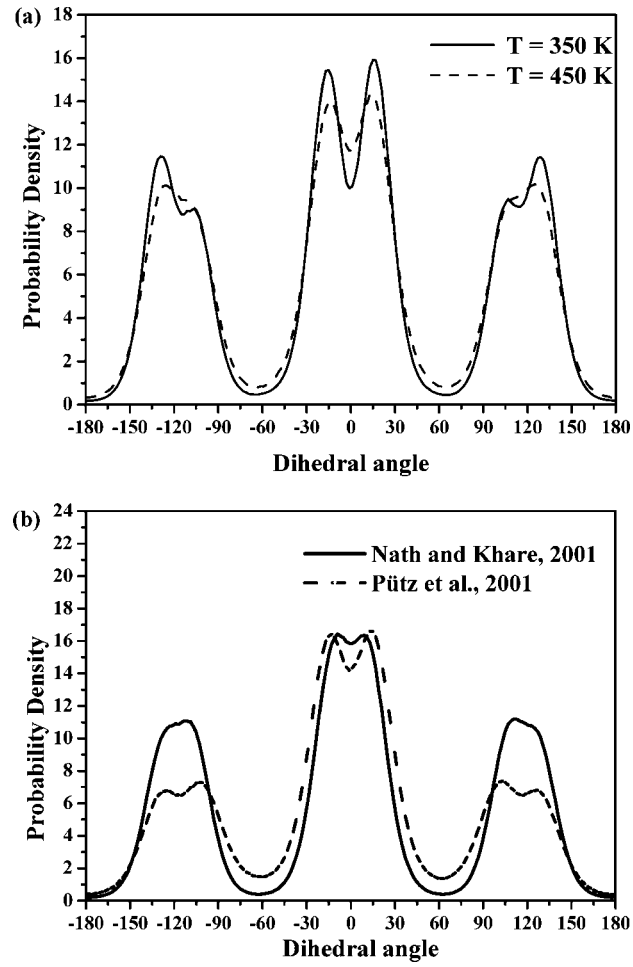

Figure 4. (a) MD predictions for the distribution of the torsion angles, ϕ, at two different temperatures as obtained with the new UA force field. (b) The corresponding distributions at $T = 450$ K if the MD simulations had been executed with the force fields proposed by Nath and Khare[42] (solid line) and by Pütz et al.[7] (dashed line).

Table 3. MD Predictions for the Mean-Square End-to-End Distance, $\langle R^2 \rangle$, the Mean-Square Radius of Gyration, $\langle R_g^2 \rangle$, and Their Ratio, at 450 K

system	$\langle R^2 \rangle$ (Å^2)	$\langle R_g^2 \rangle$ (Å^2)	$\langle R^2 \rangle / \langle R_g^2 \rangle$
C_{32}	151 ± 10	26 ± 1	5.8 ± 0.2
C_{48}	264 ± 10	44 ± 2	6.0 ± 0.2
C_{64}	384 ± 20	65 ± 2	5.9 ± 0.3
C_{80}	495 ± 20	80 ± 4	6.2 ± 0.3
C_{100}	643 ± 20	105 ± 5	6.1 ± 0.3
C_{120}	805 ± 50	135 ± 10	6.1 ± 0.4
C_{140}	950 ± 50	150 ± 10	6.3 ± 0.4
C_{160}	1100 ± 100	188 ± 10	5.8 ± 0.5
C_{200}	1400 ± 100	230 ± 15	6.1 ± 0.3
C_{240}	1700 ± 150	270 ± 20	6.2 ± 0.4
C_{320}	2200 ± 200	385 ± 30	5.7 ± 0.5

For example, in Figure 4b we show the predictions for the distribution of torsion angles at 450 K as obtained with the Nath and Khare[42] (solid line) and the Pütz et al.[7] (dashed line) force fields. We observe that the Nath and Khare[42] model practically fails to predict the six characteristic conformational states while the Pütz et al.[7] model underestimates the population of gauche states.

In Table 3, we report MD predictions for the mean-square end-to-end distance, $\langle R^2 \rangle$, and the average radius of gyration, $\langle R_g^2 \rangle$, of PIB as a function of chain length at 450 K. We also report the ratio $\langle R^2 \rangle / \langle R_g^2 \rangle$; for all systems, this assumes values practically between 5.8 and 6.2, thus confirming within the simulation error the validity of Flory's random coil hypothesis.

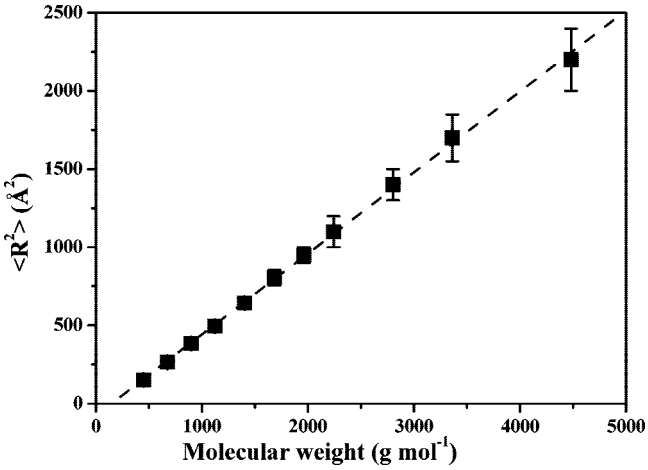

Figure 5. Variation of the chain mean-square end-to-end distance, $\langle R^2 \rangle$, with molecular weight, M, at 450 K.

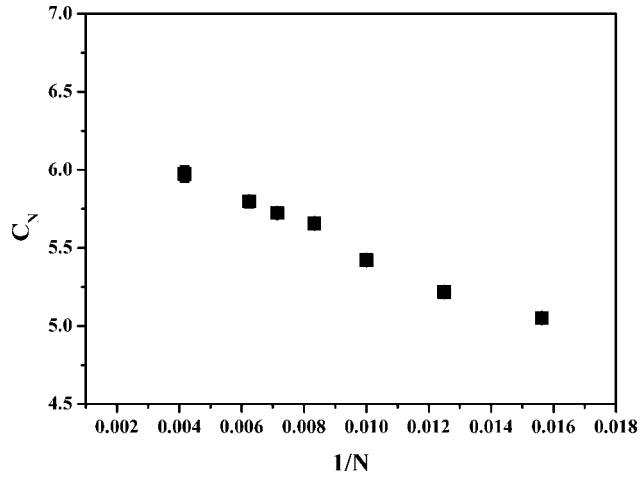

Figure 6. Variation of the characteristic ratio, C_N, with the inverse of the number of carbon atoms per chain, $1/N$, at 450 K.

In Figure 5, on the other hand, we report MD simulation results for the molecular weight (M) dependence of $\langle R^2 \rangle$ in PIB melts at 450 K. Consistent with many other polymer systems (such as the *cis*-1,4-PB[53] and *cis*-1,4-polyisoprene[54]), the dimensions of long enough PIB chains increase linearly with MW. The best linear fit to the simulation data indicates then that

$$\frac{\langle R^2 \rangle}{M} = 0.52 \text{ Å}^2 \text{ mol g}^{-1} \quad (5)$$

which agrees favorably with the value $\langle R^2 \rangle / M = 0.57$ Å^2 mol g^{-1} reported by Aharoni.[55] From the chain length dependence of $\langle R^2 \rangle$, an estimate of the characteristic ratio C_N for PIB, defined as $C_N = \langle R^2 \rangle / (N/2) l^2$, where N is the number of carbon atoms per chain and $l = 1.54$ Å, is extracted. In particular, by plotting C_N as a function of the inverse number of carbon atoms N per chain (see Figure 6), fitting the simulation results with a polynomial, and extrapolating to infinite chain length, an estimate for C_∞ can be extracted. The value thus obtained is $C_\infty = 6.3 \pm 0.1$, which agrees very satisfactorily with the experimental measurements of Ferry and Parks[56] ($C_\infty = 6.6$), Fox and Flory[57] ($C_\infty = 6.6$), Fetters et al.[24,58] ($C_\infty = 6.8$), and Hayashi et al.[8] ($C_\infty = 6.8$) as well as the theoretical calculations of Allegra et al.[59] ($C_\infty = 6.4-6.75$), Boyd and Breitling[29] ($C_\infty = 4.59$), Lohse[60] ($C_\infty = 6.73$), Weinhold et al.[6] ($C_\infty = 7.1$), and Suter et al.[30,31] ($C_\infty = 6.6$).

3.3. Structural Properties. The results presented in section 3.2 showed that the new UA model reproduces the conformational (end-to-end distance) properties of PIB rather accurately over a wide range of temperatures. A remaining question is how well it predicts the structural properties of PIB, as quantified for example by the intermolecular pair distribution function, $g(r)$. In Figure 7a, $g(r)$ predictions are shown for three different PIB systems (C_{80}, C_{100}, C_{160}) at 450 K. In all cases, simulation results exhibit two rather broad peaks at ~8 and 15 Å

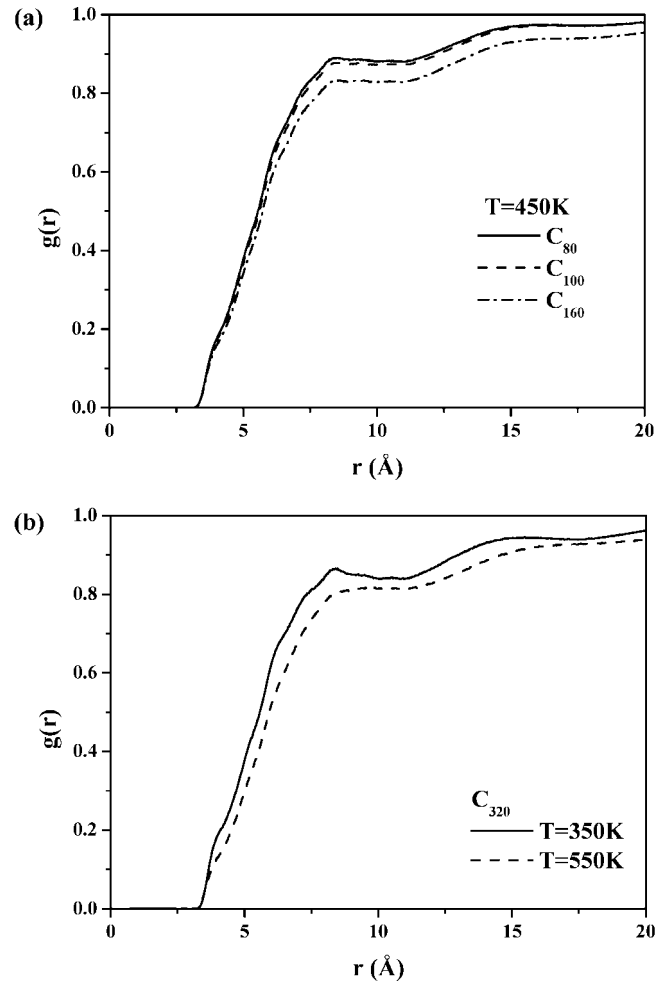

Figure 7. (a) Intermolecular pair distribution function, $g(r)$, for the C_{80}, C_{100}, and C_{160} PIB systems at 450 K. (b) Intermolecular pair distribution function, $g(r)$, for the C_{320} PIB system at 350 and 550 K.

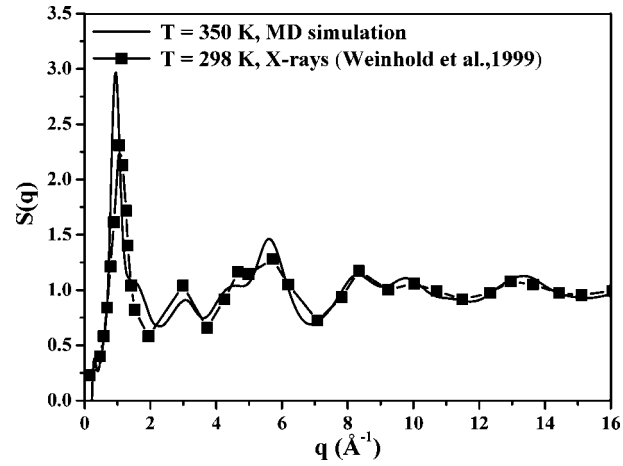

Figure 8. X-ray diffraction patterns of PIB from MD simulations at 350 K (solid line) and experiment (ref 6) at 298 K (symbols).

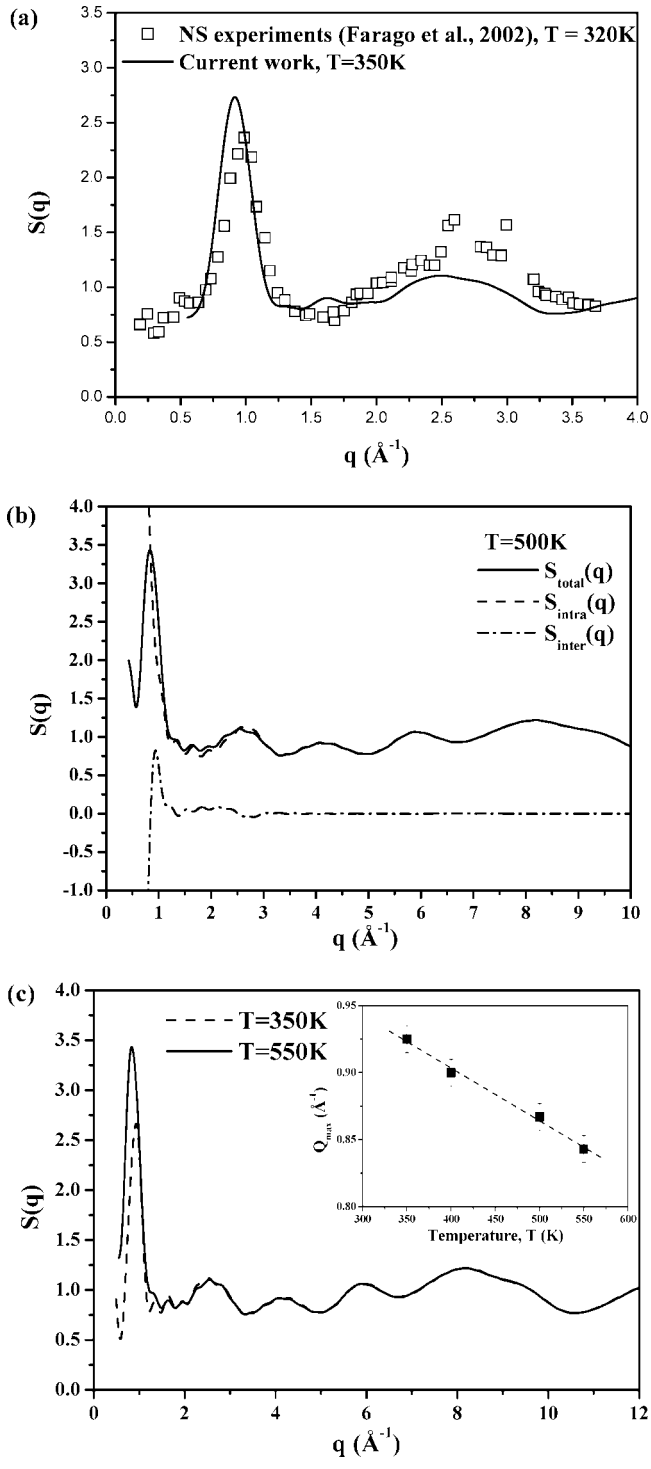

Figure 9. (a) Static structure factor, $S(q)$, as obtained from the present MD simulations at 350 K (solid line) and comparison with the NS data of ref 12 (symbols) at 320 K. (b) Intra- and intermolecular contributions to $S(q)$ at 500 K. (c) Static structure factor, $S(q)$, as obtained from the present MD simulations at 350 and 550 K and the dependence of its first peak position, Q_{max}, to temperature.

characteristic of local packing in PIB as well as the so-called "correlation hole effect" which persists over distances commensurate with the radius of gyration of the chain. It is also seen that as the chain length increases, the position of the first peak shifts smoothly toward lower distances, reflecting the increase in the density of the melt at higher MW values. The same happens if the temperature is decreased (see Figure 7b).

The total pair distribution function, $g_{total}(r)$, defined as the sum of the intermolecular pair distribution and intrachain pair density functions is directly related to the static structure factor, $S(q)$, through the following Fourier transform:

$$S(q) = 1 + \rho n \int_0^\infty 4\pi r^2 \frac{\sin(qr)}{qr}[g_{total}(r) - 1]\, dr \qquad (6)$$

where n is the total number of atoms in the system, q the magnitude of the scattering vector, and ρ the system density. $S(q)$ can be measured experimentally either by X-ray or NS. The $S(q)$ vs q plots were found to be practically the same for all PIB systems studied, so in Figure 8 only the curve corresponding to the C_{320} system at 350 K is reported together with the X-ray experimental results of Weinhold et al.[6] at 298 K. The agreement between the two curves is very good. Simulations capture accurately the first sharp peak at around 1 Å^{-1} that is attributed mostly to intermolecular correlations. They are also able to capture the other characteristic peaks at progressively larger q values (corresponding to shorter characteristic distances along the PIB chains) reflecting intramolecular correlations.

An additional comparison has been made against reported NS experimental data for deuterated PIB. To this end, it was necessary to account for the existence of different species in the polymer system and calculate $S(q)$ from the Fourier transform of the weighted pair distribution function $H(r)$, defined as[61,62]

$$H(r) = \sum_{i=1}^{2}\sum_{j=1}^{2} \frac{x_i x_j f_i f_j}{\left(\sum_{i=1}^{2} x_i f_i\right)^2}(g_{ij} - 1) \qquad (7)$$

where x_i and x_j denote the number fractions of i-type and j-type atoms in the system and f_i and f_j their corresponding scattering factors. To complete the calculations, the UA model was mapped onto an AA model by placing explicitly hydrogen atoms in all PIB chains in the simulation cell and by using the scattering vector of deuteron (instead of hydrogen) in eq 7. Results are shown in Figure 9a: The solid line represents the simulation data at 350 K and the symbols the NS experimental data[12] at 320 K. The overall agreement between the two sets of data is satisfactory, in particular with respect to the location and intensity of the first sharp peak at ~1 Å^{-1}. A relatively small difference is observed in the intensity of the second peak.

In Figure 9b, the total structure factor is analyzed in terms of intra- and intermolecular contributions. With the exception of the first peak to which both inter- and intramolecular correlations contribute significantly, all other peaks are clearly of intramolecular origin. Figure 9c, on the other hand, depicts MD simulation results for the $S(q)$ profiles at two different temperatures, 350 and 550 K, following the procedure described above. It is clear that temperature changes affect the position and intensity only of the first peak. More precisely, the intensity of the first peak, Q_{max}, increases with temperature, while its position shifts to lower q values (i.e., to larger distances) reflecting the decrease in the density of PIB. This is demonstrated at the inset of Figure 9c, where Q_{max} is plotted as a function of T and the results are seen to fall on a straight line. The data of Figure 9c can be further used to deduce the "linear thermal expansion coefficient" β of PIB defined as

$$\beta = (1/Q_{max})(\partial Q_{max}/\partial T)_P \qquad (8)$$

The simulation prediction of $\beta = (4.4 \pm 0.3) \times 10^{-4}K^{-1}$ compares favorably with the experimental value of $5.0 \times 10^{-4}K^{-1}$ based on NS measurements.[12]

3.4. Thermodynamic Properties. In Figure 10, the specific volume, v, of PIB melt at 450 K with respect to chain length N

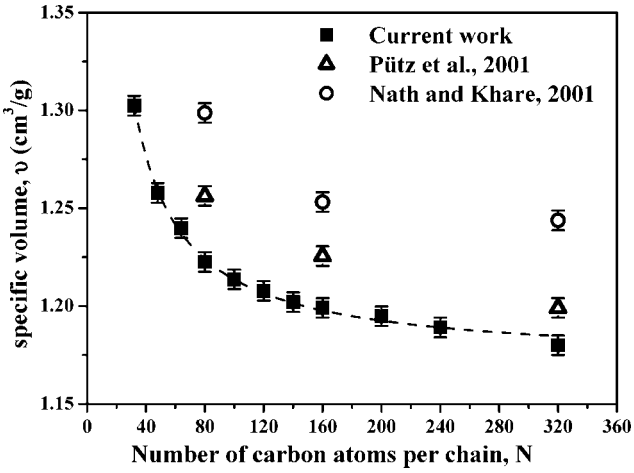

Figure 10. Dependence of the specific volume, v, on chain length, N. The dashed line shows the hyperbolic fit (eq 9) to the simulation data. Open symbols indicate the values of v that would have been obtained if the MD simulations had been executed with the force fields proposed by Nath and Khare[42] (circles) and Pütz et al.[7] (triangles).

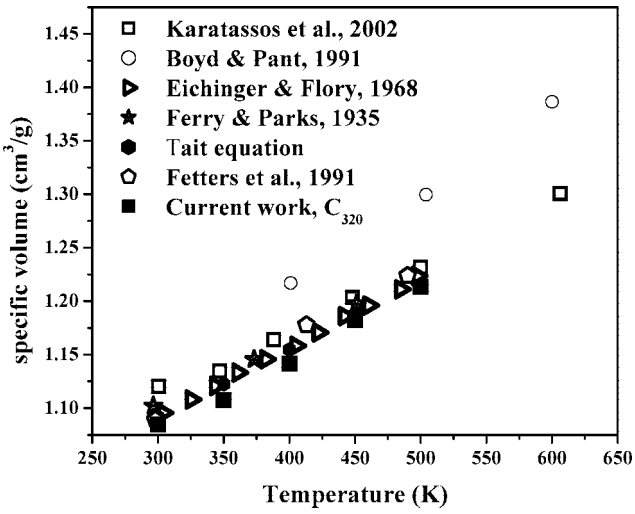

Figure 11. Temperature dependence of the specific volume, v, for the C_{320} PIB system. Filled symbols refer to MD simulation results from this work. Open symbols represent available experimental[24,56,63] and simulation[3,20] data in the literature and the predictions of the Tait equation.[64,65]

Table 4. Experimental Data and MD Predictions from This Work and from Literature for the Thermal Expansion Coefficient, α_P

T (K)	α_P ($\times 10^{-4}$) (K^{-1})	reference
300	6.06	current work
400	5.75	current work
294	6.03	Kilburn et al.[23]
296	5.2	Anderson et al.[66]
400	5.7	Eichinger and Flory[63]
400	5.7	Simha and Boyer[67]
400	5.1	Karatasos et al.[34]

is presented. MD simulation data (filled symbols) are fitted very accurately with a hyperbolic function of the form

$$v = v_\infty + \frac{v_0}{N} \tag{9}$$

Equation 9 describes both the monotonic decrease of v with N and its asymptotic behavior in the limit of high N (dashed curve). At 450 K, the best fit to simulation data results in $v_\infty = 1.171$ cm^3/g and $v_0 = 2.103$ cm^3/g. According to the experimental data of Eichinger and Flory,[63] the specific volume of high molecular weight PIB at different temperatures is described by the equation

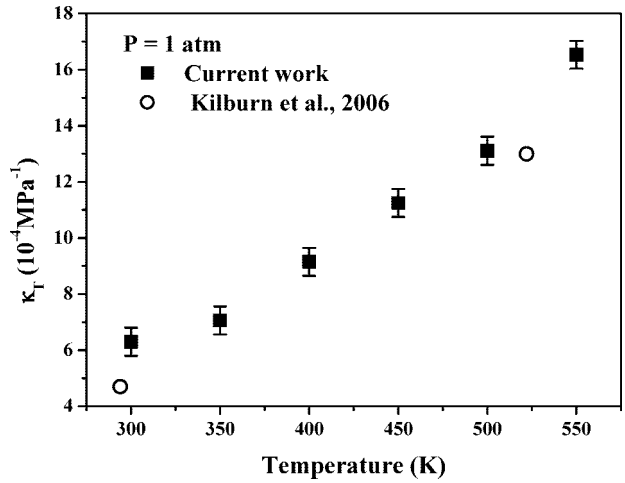

Figure 12. Temperature dependence of the isothermal compressibility, κ_T, as calculated from the present MD simulations using eq 12 (closed symbols) and comparison with experimental data[23] (open symbols).

$$v_\infty(T) = (0.9297 - 5.123\times10^{-4}T + 6.15\times10^{-4}T)^{-1} \tag{10}$$

where T is measured in °C. At 450 K, this equation yields $v_\infty = 1.189$ cm^3/g, which is only 1.5% higher than the value predicted by the present MD simulations. A similar value of $v_\infty = 1.188$ cm^3/g is extracted when one invokes the empirical Tait equation of state to fit experimental data, as proposed by Beret and Prausnitz[64] and Rodgers.[65]

For comparison, also shown in Figure 10 (with the open symbols) are the predictions of the MD simulations for the specific volume of three of the PIB systems (C_{80}, C_{160}, and C_{320}) based on the force fields proposed by Nath and Khare[42] and Pütz et al.[7] The figure shows that both models significantly overpredict the specific volume, the largest deviations (up to 8% in some cases) being exhibited by the Nath and Khare[42] molecular model.

The specific volume, v, of PIB was calculated over a wide temperature range and compared against experimental data and predictions from previous simulation work. In Figure 11, MD results for the C_{320} PIB melt (filled symbols) are compared to literature reported values (open symbols).[3,20,24,56,63–65] The difference between current simulation results and experimental data is always less than 2−3% over the studied temperature range.

The linear variation of specific volume with temperature permits a reliable estimate of the thermal expansion coefficient of PIB, α_P, according to the expression

$$\alpha_P = \frac{1}{v}\left(\frac{\partial v}{\partial T}\right)_P \tag{11}$$

and its temperature dependence. The results are summarized in Table 4 together with experimentally measured values for comparison.[23,34,63,66,67] The overall agreement between simulation and experiments is satisfactory, except from the data of Anderson et al.[66] which indicate a somewhat lower value for α_P. It should be also noted that α_P increases as T decreases at ambient pressure. A similar behavior has been reported recently for *cis*-1,4-polybutadiene.[62]

In Figure 12, simulation predictions are presented for the isothermal compressibility, κ_T, as a function of temperature. κ_T is easily calculated from the fluctuations in the system volume recorded in the course of *NPT* MD simulations according to

Table 5. UA Force Field Parameters for the Light Gases

gas	σ (Å)	ε (kcal mol^{-1})	l_0 (Å)
He[a]	3.11	0.008	
Ar[b]	3.41	0.236	
N_2[c]	3.31	0.071	1.10
O_2[d,e]	3.09	0.089	1.21

[a] Taken from ref 68. [b] Taken from ref 69. [c] Taken from ref 70. [d] Taken from ref 71. [e] Taken from ref 72.

$$\kappa_T = \frac{\langle V^2\rangle - \langle V\rangle^2}{k_B T\langle V\rangle} \tag{12}$$

Experimental data from the work of Kilburn et al.[23] are also shown in Figure 12. The two sets of data are consistent with each other. It is observed that κ_T decreases with decreasing temperature, reflecting the decreasing rate of compression at lower temperatures. We should mention here that Anderson et al.[66] have also reported a value of κ_T ($= 3.65 \times 10^{-4}$ MPa^{-1} at 296 K) which deviates from the data of Figure 12.

4. Solubility of PIB to Small Molecules

For the calculation of the barrier properties of a polymer, a realistic atomistic representation of the polymer matrix and of the penetrant molecules is required. In this work, the solubility of four light gases (He, Ar, N_2, and O_2) in PIB has been examined. The LJ parameters for He were taken from ref 68 based on simulation data fitted to vapor−liquid equilibria, while those for Ar were obtained from Hirschfelder et al.[69] based on fittings of simulation data to second virial coefficient data. N_2 and O_2 were modeled as diatomic molecules with constant bond length using the potential model proposed by Potoff and Siepmann[70] for N_2 fitted to VLE data and the potential model proposed by Huber and Herzberg[71] and Powles and Gubbins[72] for O_2. Details on model parameters are given in Table 5. The standard Lorentz−Berthelot combining rules were used for the LJ interactions between unlike polymer−gas molecules. The LJ potential beyond $r = 1.45\sigma$ was substituted by a fifth-order polynomial, whose value beyond $r = 2.3\sigma$ was set equal to zero. The tail contributions to the internal energy were taken into account according to the method described by Allen and Tildesley[73] (eq 2.136 in ref 73).

The infinite dilution solubility coefficient, S_0, of a gas in PIB was calculated based on Widom's test particle insertion technique.[74] According to this method, a "ghost" molecule is inserted at a random position in the simulated system and its interaction energy, U_{ghost}, with the surrounding atoms of the polymer matrix is computed. In the *NPT* statistical ensemble, the excess chemical potential μ^{ex} of the inserted molecule is calculated through the expression[75]

$$\begin{aligned}\mu^{ex} &= \mu - \mu^{ig} \\ &= -\frac{1}{\beta}\ln\left[\frac{1}{\langle V\rangle_{NPT}}\langle V\langle\exp(-\beta U_{ghost}^{intra} - \beta U_{ghost}^{inter})\rangle_{Widom}\rangle_{NPT}\right] + \\ &\quad \frac{1}{\beta}\ln\langle\exp(-\beta U_{ghost}^{intra})\rangle_{ideal\ gas}\end{aligned} \tag{13}$$

where U_{ghost}^{inter} and U_{ghost}^{intra} stand for the inter- and intramolecular contributions, respectively, to U_{ghost}. In this work, only spherical and rigid diatomic gas molecules have been examined; therefore, U_{ghost}^{intra} was in all cases set equal to zero. In eq 13, $\beta = 1/k_B T$, where k_B is Boltzmann's constant, V is the instantaneous volume of the system, and the brackets denote statistical mechanical (i.e., ensemble) averages over all possible polymer matrix configurations and all possible positions of the "ghost" molecule. Once the excess chemical potential has been calculated, S_0 is obtained through

$$S_0 = \frac{22400\ \text{cm}^3\ (\text{STP})/\text{mol}}{RT}\lim_{x_{solute}\to 0}\exp(-\beta\mu_{solute}^{ex}) \tag{14}$$

and is expressed in units of cm^3 (STP)/(cm^3 Pa) with STP corresponding to an absolute pressure of 101.325 kPa and a temperature of 273.15 K.

S_0 calculations for the various gases in different temperatures are shown in Table 6, while in Figure 13 these results are compared against experimental data from van Amerongen[76] for He, O_2, and N_2 and predictions from an accurate macroscopic model[77] used widely for engineering calculations involving Ar. For the case of He, the agreement between experimental data and simulation predictions is excellent. In all other cases, the MD calculations with the employed UA force fields for the matrix and the solute systematically overpredict the experimental data. It is encouraging though that the employed UA model for PIB captures correctly the temperature effect on S_0. It predicts that the solubility of Ar and O_2 in PIB decreases with temperature while the solubility of He increases and the solubility of N_2 is practically temperature independent, in agreement with the experimental measurements. Finally, it must be noted that in the case of O_2 molecules additional solubility calculations were preformed using the VLE-based parameters obtained from Zhang and Siepmann.[78] Solubility predictions with this model were somewhat higher than the values presented in Figure 13 and are not reported here.

Motivated by the failure of the UA model to quantitatively predict the solubility of Ar, O_2, and N_2 in PIB, we adopted a more detailed all-atom (AA) atomistic representation of PIB chains. To this end, the very detailed and accurate COMPASS (= condensed-phase optimized molecular potentials for atomistic simulation studies) force field involving 13 terms in the expression for the potential energy was employed in the solubility calculations.[79] The consideration of an explicit atom model underlies the essential step in the accurate prediction of permeability and barrier properties because by directly considering hydrogen atoms permits a more detailed representation of small polymer matrix cavities in the simulation cell that are significant for gas molecule solubility. Furthermore, hydrogen atoms exhibit enhanced mobility, causing an increase in the dynamic flexibility of the system through the fast local rearrangements of the accessible volume which is particularly important for the diffusion of small gas molecules.

In the present work, a certain number of uncorrelated PIB configurations were selected from the accumulated MD trajectories with the new UA model and converted to AA PIB structures by considering also the hydrogen atoms on the carbon atoms of PIB chains (see Figure 14). Of course, the conversion

Table 6. MD Simulation Results for the Solubility S_0 of the Four Light Gases in PIB

	S_0 ($\times 10^6$ cm^3 (STP)/cm^3 Pa)							
	He		Ar		O_2		N_2	
T (K)	UA	AA	UA	AA	UA	AA	UA	AA
300	0.16 ± 0.02	0.23 ± 0.01	2.10 ± 0.06	1.38 ± 0.09	1.63 ± 0.07	1.1 ± 0.1	0.98 ± 0.05	0.31 ± 0.06
350	0.24 ± 0.01	0.25 ± 0.01	1.80 ± 0.05	1.1 ± 0.1	1.47 ± 0.07	0.9 ± 0.1	0.98 ± 0.05	0.25 ± 0.07
400	0.32 ± 0.01		1.67 ± 0.05	1.04 ± 0.08	1.30 ± 0.05		0.95 ± 0.02	
450	0.39 ± 0.01	0.36 ± 0.02	1.54 ± 0.02	1.01 ± 0.07	1.27 ± 0.03	0.7 ± 0.1	0.96 ± 0.03	0.31 ± 0.07
500	0.47 ± 0.01	0.39 ± 0.02	1.44 ± 0.02	0.92 ± 0.05	1.26 ± 0.02	0.67 ± 0.07	0.95 ± 0.01	0.34 ± 0.05
550	0.56 ± 0.01	0.47 ± 0.02	1.41 ± 0.01	0.93 ± 0.03	1.21 ± 0.01	0.57 ± 0.07	0.99 ± 0.01	0.35 ± 0.05
600	0.63 ± 0.01	0.55 ± 0.01	1.37 ± 0.01	0.74 ± 0.03	1.19 ± 0.01	0.52 ± 0.07	1.04 ± 0.01	0.30 ± 0.06

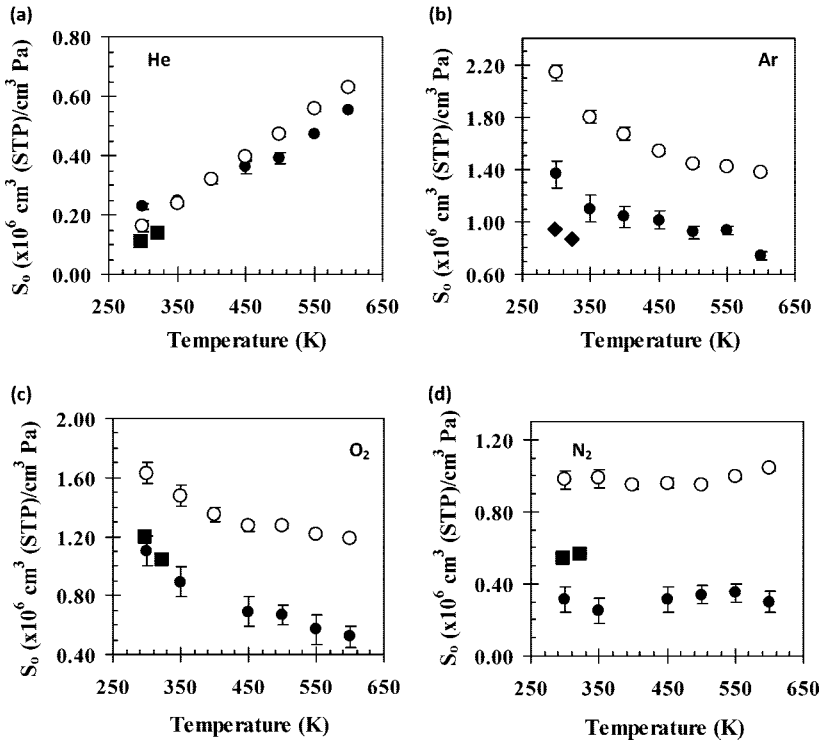

Figure 13. Infinite dilution solubility coefficient S_0 (cm^3 (STP)/cm^3 Pa) of (a) He, (b) Ar, (c) O_2, and (d) N_2 in PIB from MD simulations with the UA model (open circles) and the AA COMPASS force field (solid circles) and comparison with experimental data[76] and macroscopic model predictions.[77]

from a UA to an AA representation gives rise to steric overlaps, but these can be easily eliminated by subjecting the system to an energy minimization procedure (e.g., through a steepest descent method) followed by an extra thermal re-equilibration step through an *NVT* or *NPT* MD run for a rather short time up to a few hundreds of picoseconds. Following such a strategy using the Materials Studio software package of Accelrys Inc.,[46] we generated 10 independent and fully relaxed PIB configurations at each temperature in the range from 300 K up to 600 K from the UA simulations with the C_{240} system, which we used next to calculate S_0 for the four gases in PIB. In these calculations, the COMPASS[79] force field was also used to describe the potential energy interactions of the four gas molecules. The solubility calculations at several temperatures were carried out with the Henry constant method of Materials Studio.[46] The electrostatic interactions between polymer solutes were calculated using the Ewald summation method.[73] For the van der Waals interactions, a cubic spline was used for distances beyond 11.5 Å together with a value of 12.5 Å for the cutoff distance. Results are presented in Table 6 and Figure 13, together with experimental data and UA predictions.

The agreement between experimental data and AA predictions is excellent for He, Ar, and O_2. For the case of N_2, AA predictions are lower than experimental data but still more accurate than those based on the UA model. In all cases, the temperature effect on the solubility is captured accurately for all gases, and so experimental data, UA predictions, and AA predictions are in agreement. Temperature effects on the solubility of gases in rubbery polymers have been discussed in detail by Economou et al.[80]

In the literature, simulation results for the solubility of light gases in PIB have been reported by Müller-Plathe et al.[41] and Gusev and Suter.[81] Müller-Plathe et al.[41] calculated S_0 of He and O_2 in PIB using Widom's particle insertion technique based on an AA model, but their results exceeded the experimental data by 1−2 orders of magnitude. On the other hand, the transition state theory (TST)-based calculations of Gusev and

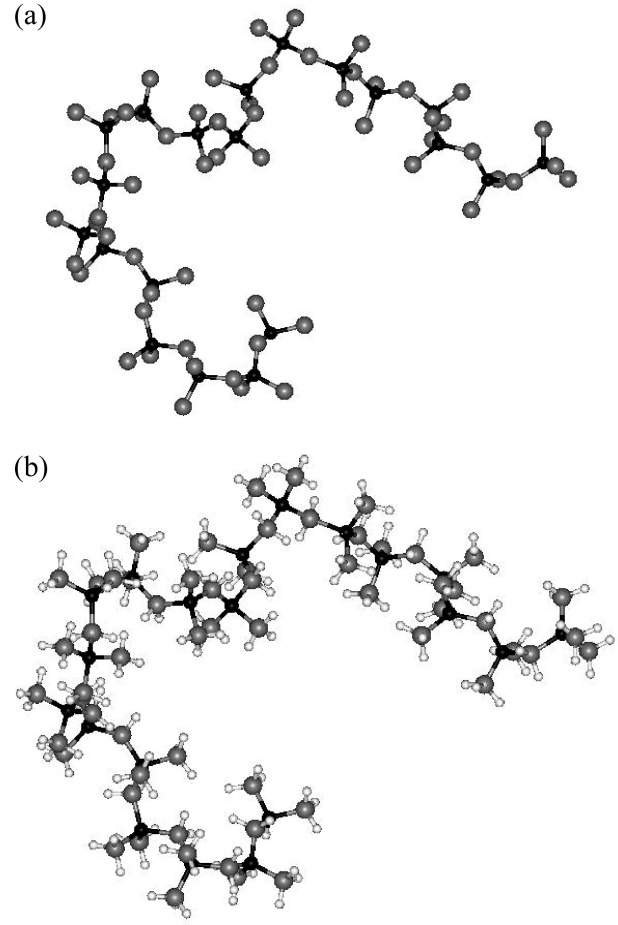

Figure 14. Typical atomistic snapshot of a fully relaxed C_{80} PIB chain from MD simulation at 350 K in the UA (a) and AA (b) representations.

Suter[81] for the solubility of He, H_2, Ar, O_2, and N_2 in PIB overestimated the experimental data of van Amerongen[76] by 10−40 times.

5. Conclusions and Future Plans

We presented results of a computer simulation study concerning the solubility of four penetrant molecules (He, Ar, O_2, and N_2) in PIB. Our simulation strategy involves the following steps: (i) equilibration of model PIB systems at various temperatures through a brute-force application of a parallel MD method based on a new UA model that correctly reproduces the volumetric, structural, and conformational properties of PIB over a range of temperatures; (ii) conversion of representative, fully equilibrated configurations from these simulations to AA PIB structures and thermal re-equilibration, and (iii) sorption computational experiments at various temperatures, for the estimation of the solubility parameter of the four penetrants in PIB. The new model, based on widely accepted interaction potentials introduced by Martin and Siepmann,[44] Nath and Khare,[42] and Poncela et al.,[45] reproduces correctly the conformational characteristics of PIB chains, in particular the splitting of the trans and gauche states, as has been suggested in the past by elaborate theories and AA simulations. Moreover, it allowed us to simulate within reasonable CPU time a number of model PIB systems of molecular length up to 320 carbon atoms per chain at several temperatures above the melting point.

Well-relaxed configurations from these simulations were used as input in simulations with the all-purpose AA COMPASS force field[79] for the prediction of the solubility of the four gases in PIB. Our results demonstrate that at room temperature O_2 is more soluble in PIB by about 2 times than N_2 and that He is less soluble than Ar by almost 1 order of magnitude. They also indicate a rapid decrease in O_2 solubility as the temperature is increased; in contrast, the solubility of N_2 remains practically unaffected. Despite this, the solubility of O_2 remains above that of N_2 for all temperatures. Similarly, the solubility of He increases rapidly with increasing temperature whereas that of Ar decreases. However, Ar remains always more soluble in PIB than He.

We also demonstrated that solubility calculations of O_2, N_2, and Ar based on well-known UA models, although qualitatively correct, significantly overestimate the experimental data and the COMPASS-based simulation results (by a factor of 4 in some cases).

Work is currently in progress to address the diffusive properties of the small penetrant molecules studied here in PIB as a function of temperature and the role of molecular packing and energetics on the barrier properties of PIB compared with other elastomeric polymers, such as (e.g.) polyethylene (PE). The microstructure of free volume as well as its temperature and pressure dependencies will also be studied. In the future, the present simulations will be extended to (a) longer systems in order to calculate the linear viscoelastic properties of PIB (friction constants, interentanglement spacing, diffusivity, and plateau modulus) and (b) significantly lower temperatures in order to determine its glass transition temperature.

Acknowledgment. Financial support of research work in "Demokritos" by the European Union−European Social Fund, the Greek Secretariat of Research and Technology, and Bayer Technology Services GmbH is gratefully acknowledged.

References and Notes

(1) Frick, B.; Richter, D.; Trevino, S. *Physica A* **1993**, *201*, 88.
(2) Angell, C. A. *Science* **1995**, *267*, 1924.
(3) Boyd, R. H.; Pant, P. V. K. *Macromolecules* **1991**, *24*, 6325.
(4) Puskas, J. E.; Chen, Y. H. *Biomacromolecules* **2004**, *5*, 1141.
(5) Londono, J. D.; Habenschuss, A.; Curro, J. G.; Rajasekaran, J. J. *J. Polym. Sci., Part B: Polym. Phys.* **1996**, *34*, 3055.
(6) Weinhold, J. D.; Curro, J. G.; Habenschuss, A.; Londono, J. D. *Macromolecules* **1999**, *32*, 7276.
(7) Pütz, M.; Curro, J. G.; Grest, G. S. *J. Chem. Phys.* **2001**, *114*, 2847.
(8) Hayashi, H.; Flory, P. J.; Wignall, G. D. *Macromolecules* **1983**, *16*, 1328.
(9) Frick, B.; Dosseh, G.; Cailliaux, A.; Alba-Simionesco, C. *Chem. Phys.* **2003**, *292*, 311.
(10) Richter, D.; Monkenbusch, M.; Arbe, A.; Colmenero, J. *J. Non-Cryst. Solids* **2001**, *287*, 286.
(11) Arrighi, V.; Triolo, A.; Qian, H. *J. Non-Cryst. Solids* **2002**, *307*, 654.
(12) Farago, B.; Arbe, A.; Colmenero, J.; Faust, R.; Buchenau, U.; Richter, D. *Phys. Rev. E* **2002**, *65*, 051803.
(13) Richter, D.; Monkenbusch, M.; Allgeier, J.; Arbe, A.; Colmenero, J.; Farago, B.; Bae, Y. C.; Faust, R. *J. Chem. Phys.* **1999**, *111*, 6107.
(14) Arbe, A.; Monkenbusch, M.; Stellbrink, J.; Richter, D.; Farago, B.; Almdal, K.; Faust, R. *Macromolecules* **2001**, *34*, 1281.
(15) Tanaka, A.; Ishida, Y. *J. Polym. Sci., Part B: Polym. Phys.* **1974**, *12*, 1283.
(16) Richter, D.; Arbe, A.; Colmenero, J.; Monkenbusch, M.; Farago, B.; Faust, R. *Macromolecules* **1998**, *31*, 1133.
(17) Bandis, A.; Wen, W. Y.; Jones, E. B.; Kaskan, P.; Zhu, Y.; Jones, A. A.; Inglefield, P. T.; Bendler, J. T. *J. Polym. Sci., Part B: Polym. Phys.* **1994**, *32*, 1707.
(18) Delabatie, R. D.; Laupretre, F.; Monnerie, L. *Macromolecules* **1989**, *22*, 2617.
(19) Dong, Z. P.; Cauley, B. J.; Bandis, A.; Mou, C. W.; Inglefield, C. E.; Jones, A. A.; Inglefield, P. T.; Wen, W. Y. *J. Polym. Sci., Part B: Polym. Phys.* **1993**, *31*, 1213.
(20) Karatasos, K.; Ryckaert, J. P.; Ricciardi, R.; Laupretre, F. *Macromolecules* **2002**, *35*, 1451.
(21) McGrath, K. J.; Ngai, K. L.; Roland, C. M. *Macromolecules* **1992**, *25*, 4911.
(22) Rizos, A. K.; Ngai, K. L.; Plazek, D. J. *Polymer* **1997**, *38*, 6103.
(23) Kilburn, D.; Wawryszczuk, J.; Dlubek, G.; Pionteck, J.; Hassler, R.; Alam, M. A. *Macromol. Chem. Phys.* **2006**, *207*, 721.
(24) Fetters, L. J.; Graessley, W. W.; Kiss, A. D. *Macromolecules* **1991**, *24*, 3136.
(25) Ngai, K. L.; Plazek, D. J.; Echeverria, I. *Macromolecules* **1996**, *29*, 7937.
(26) Plazek, D. J.; Chay, I. C.; Ngai, K. L.; Roland, C. M. *Macromolecules* **1995**, *28*, 6432.
(27) Hoeve, C. A. *J. Chem. Phys.* **1960**, *32*, 888.
(28) Madkour, T. M.; Mohammed, O. I.; Ebaid, A. H. *J. Macromol. Sci., Phys.* **2000**, *B39*, 679.
(29) Boyd, R. H.; Breitling, S. M. *Macromolecules* **1972**, *5*, 1.
(30) Suter, U. W.; Saiz, E.; Flory, P. J. *Macromolecules* **1983**, *16*, 1317.
(31) Debolt, L. C.; Suter, U. W. *Macromolecules* **1987**, *20*, 1424.
(32) Vacatello, M.; Yoon, D. Y. *Macromolecules* **1992**, *25*, 2502.
(33) Karatasos, K.; Ryckaert, J. P. *Macromolecules* **2001**, *34*, 7232.
(34) Karatasos, K.; Saija, F.; Ryckaert, J. P. *Physica B* **2001**, *301*, 119.
(35) Pant, P. V. K.; Boyd, R. H. *Macromolecules* **1993**, *26*, 679.
(36) Han, J.; Boyd, R. H. *Macromolecules* **1994**, *27*, 5365.
(37) Han, J.; Gee, R. H.; Boyd, R. H. *Macromolecules* **1994**, *27*, 7781.
(38) Cho, D. W.; Neuburger, N. A.; Mattice, W. L. *Macromolecules* **1992**, *25*, 322.
(39) Müller-Plathe, F.; Rogers, S. C.; Vangunsteren, W. F. *Macromolecules* **1992**, *25*, 6722.
(40) Müller-Plathe, F.; Rogers, S. C.; Vangunsteren, W. F. *Chem. Phys. Lett.* **1992**, *199*, 237.
(41) Müller- Plathe, F.; Rogers, S. C.; Vangunsteren, W. F. *J. Chem. Phys.* **1993**, *98*, 9895.
(42) Nath, S. K.; Khare, R. *J. Chem. Phys.* **2001**, *115*, 10837.
(43) Gee, R. H.; Boyd, R. H. *Polymer* **1995**, *36*, 1435.
(44) Martin, M. G.; Siepmann, J. I. *J. Phys. Chem. B* **1999**, *103*, 4508.
(45) Poncela, A.; Rubio, A. M.; Freire, J. J. *Mol. Phys.* **1997**, *91*, 189.
(46) Materials Studio, M. S. P., Accelrys Software Inc., San Diego, CA.
(47) Nosé, S. *Prog. Theor. Phys. Suppl.* **1991**, *103*, 1.
(48) Hoover, W. G. *Rhys. Rev. A* **1985**, *31*, 1695.
(49) Ryckaert, J. P.; Ciccotti, G.; Berendsen, H. J. C. *J. Comput. Phys.* **1977**, *23*, 327.
(50) Andersen, H. C. *J. Comput. Phys.* **1983**, *52*, 24.
(51) Plimpton, S. *J. Comput. Phys.* **1995**, *117*, 1.
(52) Tanaka, T.; Chatani, Y.; Tadokoro, H. *J. Polym. Sci., Part B: Polym. Phys.* **1974**, *12*, 515.
(53) Gestoso, P.; Nicol, E.; Doxastakis, M.; Theodorou, D. N. *Macromolecules* **2003**, *36*, 6925.
(54) Doxastakis, M.; Mavrantzas, V. G.; Theodorou, D. N. *J. Chem. Phys.* **2001**, *115*, 11339.
(55) Aharoni, S. M. *Makromol. Chem.* **1978**, *179*, 1867.
(56) Ferry, J. D.; Parks, G. S. *Physics* **1935**, *6*, 356.
(57) Fox, T. G.; Flory, P. J. *J. Am. Chem. Soc.* **1951**, *73*, 1909.

(58) Fetters, L. J.; Hadjichristidis, N.; Lindner, J. S.; Mays, J. W.; Wilson, W. W. *Macromolecules* **1991**, *24*, 3127.
(59) Allegra, G.; Benedetti, E.; Pedone, C. *Macromolecules* **1970**, *3*, 727.
(60) Lohse, D. J. *J. Macromol. Sci., Polym. Rev.* **2005**, *C45*, 289.
(61) Tsolou, G.; Mavrantzas, V. G.; Theodorou, D. N. *Macromolecules* **2005**, *38*, 1478.
(62) Tsolou, G.; Harmandaris, V. A.; Mavrantzas, V. G. *Macromol. Theory Simul.* **2006**, *15*, 381.
(63) Eichinger, B. E.; Flory, P. J. *Macromolecules* **1968**, *1*, 285.
(64) Beret, S.; Prausnitz, J. M. *Macromolecules* **1975**, *8*, 536.
(65) Rodgers, P. A. *J. Appl. Polym. Sci.* **1993**, *48*, 1061.
(66) Anderson, J. E.; Davis, D. D.; Slichter, W. P. *Macromolecules* **1969**, *2*, 166.
(67) Simha, R.; Boyer, R. F. *J. Chem. Phys.* **1962**, *37*, 1003.
(68) Martin, M. G.; Siepmann, J. I. *J. Phys. Chem. B* **1999**, *103*, 11191.
(69) Hirschfelder, J. O.; Curtiss, C. F.; Bird, R. B. *Molecular Theory of Gases and Liquids*; Wiley: New York, 1954.
(70) Potoff, J. J.; Siepmann, J. I. *AIChE J.* **2001**, *47*, 1676.
(71) Huber, K. P.; Herzberg, G. *Spectra and Molecular Structure IV. Constants of Diatomic Molecules*; Van Nostrand Reinhold Co.: New York, 1979.
(72) Powles, J. G.; Gubbins, K. E. *Chem. Phys. Lett.* **1976**, *38*, 405.
(73) Allen, M. P.; Tildesley, D. J. *Computer Simulation of Liquids*; Oxford Science Publications: Oxford, UK, 1987.
(74) Widom, B. *J. Chem. Phys.* **1963**, *39*, 2808.
(75) Spyriouni, T.; Economou, I. G.; Theodorou, D. N. *Macromolecules* **1997**, *30*, 4744.
(76) van Amerongen, G. J. *J. Polym. Sci.* **1950**, *5*, 307.
(77) Thorlaksen, P.; Abildskov, J.; Kontogeorgis, G. M. *Fluid Phase Equilib.* **2003**, *211*, 17.
(78) Zhang, L.; Siepmann, J. I. *Theor. Chim. Acta* **2006**, *115*, 391.
(79) Sun, H. J. *J. Phys. Chem. B* **1998**, *102*, 7338.
(80) Economou, I. G.; Makrodimitri, Z. A.; Kontogeorgis, G. M.; Tihic, A. *Mol. Simul.* **2007**, *33*, 851.
(81) Gusev, A. A.; Suter, U. W. *J. Chem. Phys.* **1993**, *99*, 2228.

MA8007652